RSC Advances

PAPER

Cite this: *RSC Adv.*, 2016, **6**, 77489

# Effect of alloying elements on the ideal strength and charge redistribution of γ′-$Ni_3Al$: a first-principles study of tensile deformation

Minru Wen[a] and Chong-Yu Wang*[ab]

Received 19th July 2016
Accepted 11th August 2016
DOI: 10.1039/c6ra13017h

The ideal strength, which is the minimum stress required to yield a perfect crystal, is fundamental for understanding the mechanical properties of real materials. Using density functional theory, the effect of the alloying elements Ta, W, Re, Mo, and Co on the ideal tensile strength ($\sigma_{IT}$) of γ′-$Ni_3Al$ along three characteristic directions was investigated. By examining the crystal mechanical stability in terms of Born criteria at every single strain during the tensile tests, the $\sigma_{IT}$ values of $L1_2$-$Ni_3Al$ along the [001], [110] and [111] directions are determined to be 12.93 GPa, 7.20 GPa and 25.55 GPa, respectively. The effect of alloying elements on $\sigma_{IT}$ shows obvious directionality because of directional interactions between impurities and host atoms. Doping with Ta, W, Re, Mo, and Co increases $\sigma_{IT}$ in the [110] direction by 13%, 18%, 21%, 17%, and 5%, respectively. Furthermore, the electronic mechanism underlying the strengthening effect of alloying elements is determined by analyzing the d-orbital partial density of states and charge redistribution.

## 1. Introduction

The ideal strength of a material is the minimum stress required to yield a perfect (defect-free) crystal and sets an upper bound for the strength of real materials.[1,2] Clearly, knowledge of the ideal strength, which is dominated by the behavior of valence electrons and ions, is fundamental for understanding the mechanical properties of materials and for development of practical applications. The strength experimentally observed in nanoindentation of a defect-free crystal can quantitatively agree with the value obtained by *ab initio* calculations.[3,4]

With advances in computational methods and modern computers, the ideal strength can be obtained by first-principles calculations.[2,5–7] Early studies focused on the ideal strength of perfect crystals, such as single crystals (*e.g.*, Al, Cu, Fe, and Ni)[2,8–12] and ordered compound systems (*e.g.*, FeAl, $Co_3$(Al,W), and SiN).[13–15] Calculation of the ideal strength has attracted great interest because it plays a crucial role in research of superhard synthesized materials.[16–19] Furthermore, the ideal strength test has been extended to defective systems. For example, Hu *et al.*[20] and Xu *et al.*[21] studied the ideal strength of intermetallic compounds with a point defect, Lu *et al.*[22] investigated the ideal tensile strength ($\sigma_{IT}$) of the Al grain boundary, and Yin *et al.*[23] investigated the tensile and fracture process of the TiN/VN interface. Additionally, the temperature-dependent ideal strength was investigated by Shang *et al.*[24,25] under the assumption that the effect of temperature only causes volume variation and electron–phonon and phonon–phonon interactions can be ignored.

Nickel-based single-crystal superalloys exhibit excellent elevated-temperature mechanical properties and are widely used for blade applications in advanced aeroplane engines and power-generation turbines.[26,27] In general, the γ′-$Ni_3Al$ precipitate phase with its anomalous temperature dependence of the yield stress is largely responsible for the mechanical strength of alloys and their resistance to deformation at high temperature.[28–30] Therefore, a study of the mechanical properties of γ′-$Ni_3Al$ should partially reflect the global properties of nickel-based superalloys. By adding alloying elements (*e.g.*, Ta, W, Ti, Co, Cr, Re, Mo, and Ru), modern commercial nickel-based superalloys achieve extraordinary high-temperature performance.[26,27,31,32] *Ab initio* calculations have been extensively used to investigate the influence of alloying elements on the properties of γ′-$Ni_3Al$.[33–37] However, these studies generally focus on the site preference of refractory elements in γ′-$Ni_3Al$. The ideal strength is not emphasized. In particular, no theoretical study has focused on the effect of W, Ta, Mo, and Co on the ideal tensile strength of nickel-based superalloys, although these alloying elements have a significant influence on the properties of alloys.[38–40]

In this study, we performed first-principles calculations to investigate the effect of alloying elements (Ta, W, Re, Mo, and Co) on $\sigma_{IT}$ of γ′-$Ni_3Al$ along the [001], [110] and [111] directions. The bonding nature of the alloying elements with host atoms, lattice evolution, and charge redistribution in the tensile process were analyzed.

[a]*Department of Physics, Tsinghua University, Beijing 100084, China. E-mail: cywang@mail.tsinghua.edu.cn*
[b]*Central Iron and Steel Research Institute, Beijing 100081, China*

## 2. Computational methods

For uniaxial tensile deformation, the tensile stress, $\sigma$, is given by[2]

$$\sigma = \frac{1}{V(\varepsilon)}\frac{\partial E}{\partial \varepsilon}, \quad (1)$$

where $E$ is the total energy and $V(\varepsilon)$ is the volume at the corresponding tensile strain $\varepsilon$. To simulate the stress–strain curve and determine the tensile strength, an incremental strain is imposed in the tensile direction. The atomic basis vectors perpendicular to the applied strain are simultaneously relaxed until the other stress components vanish. Furthermore, all the internal freedoms of the atom are relaxed at each step. Relaxation was performed until the forces on all of the atoms were less than 0.01 eV Å$^{-1}$.

Based on the hypothesis of a dilute alloy, we used a single-impurity model[41] to explore the strengthening effects of the alloying elements. Previous studies have shown that Ta, W, Re, and Mo prefer the Al site, whereas Co changes its site preference depending on the alloying composition in the $\gamma'$ phase.[34,36,42,43] Therefore, the model with alloying element X (X = Ta, W, Re, Mo, and Co) substituting the Al atom was used. A 64-atom 2$[1\bar{1}0]a_0 \times 2[110]a_0 \times 2[001]a_0$ supercell was used for the $\sigma_{IT}$ test of the [001] and [110] directions, and a 48-atom $2[1\bar{1}0]a_0 \times [111]a_0 \times [11\bar{2}]a_0$ supercell was used to calculate $\sigma_{IT}$ in the [111] direction, as shown in Fig. 1(a) and (b). The sizes of these two supercells can avoid interactions between doping atoms.

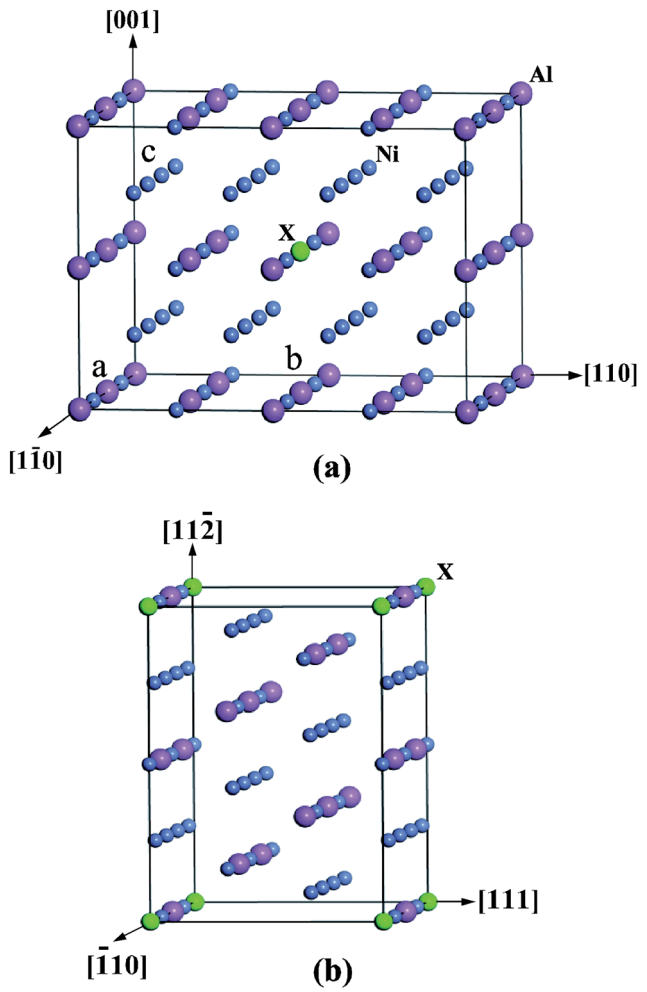


Fig. 1 (a) 64-Atom model used to test the ideal tensile processes along the [001] and [110] directions. (b) 48-Atom supercell used to test the ideal tensile processes along the [111] direction. Blue, purple, and green balls represent Ni, Al, and alloying element atom X (X = Ta, W, Re, Mo, and Co), respectively.

We used a total-energy method based on density functional theory[44,45] implemented in the Vienna Ab initio Simulation Package code.[46] The ion–electron interaction was described by the projector augmented wave method,[47] and the generalized gradient approximation of Perdew *et al.*[48] was used to describe the exchange–correction function. The plane wave cutoff was set to 350 eV. Following the Monkhorst–Pack scheme,[49] 5 × 5 × 7 and 8 × 5 × 6 $k$-point meshes were used for tensile tests of the 64-atom and 48-atom models, respectively. The energy convergence of electronic self-consistency was on the order of $10^{-5}$ eV.

Table 1 lists the calculated lattice parameter $a_0$ and elastic properties of $L1_2$-$Ni_3Al$ along with the corresponding values from experiments and other DFT calculations. Furthermore, the effects of alloying elements on the elastic properties of $\gamma'$-$Ni_3Al$ are also tabulated in Table 2. A 32-atom $2[001]a_0 \times 2[010]a_0 \times 2[100]a_0$ supercell and a 9 × 9 × 9 $k$-points mesh are used for the calculations of the elastic constants of alloying systems. The lattice parameter $a_0$ and bulk modulus $B$ are obtained by fitting the energy and volume data to the Murnaghan equation of state.[50] Under small strain, the elastic energy density of a solid is given by:[51]

$$\frac{\Delta E}{V_0} = \frac{1}{2}\sum_{i,j=1}^{6} C_{ij}\vec{e}_i\vec{e}_j, \quad (2)$$

where $\Delta E$ is the energy from the imposed strain increment having strain vector $\vec{e} = (e_1, e_2, e_3, e_4, e_5, e_6)$, $V_0$ is the equilibrium volume of the lattice cell at zero strain and $C_{ij}$ are the elastic constants. For the calculations of three independent elastic constants ($C_{11}$, $C_{12}$ and $C_{44}$) of cubic lattice, sets of distortions (as listed in Table 3) with the $\delta$ parameters varying from −0.03 to 0.03 in steps of 0.005 are employed to fit the elastic constants. $C_{11}$ and $C_{12}$ are obtained by combining $\Delta E/V_0 = 3(C_{11} - C_{12})\delta^2$ and $B = (C_{11} + 2C_{12})/3$ (relationship observed in a cubic lattice

Table 1 Calculated lattice parameter, elastic properties, and Poisson's ratio ($\nu$) of $Ni_3Al$ along with experimental and other DFT calculated values

| | Cal.[a] | Expt[b] | Expt[c] | Cal.[d] | Cal.[e] | Cal.[f] |
|---|---|---|---|---|---|---|
| $a_0$ (Å) | 3.567 | 3.57 | 3.57 | 3.568 | 3.579 | 3.56 |
| $B$ (GPa) | 175.9 | 173 | 174.3 | 174.9 | 180.4 | 185 ± 6 |
| $C_{11}$ (GPa) | 227.9 | 223 | 227 | 229.7 | 243.8 | 246 ± 6 |
| $C_{12}$ (GPa) | 149.9 | 148 | 148 | 147.5 | 148.7 | 155 ± 6 |
| $C_{44}$ (GPa) | 120.9 | 125 | 120 | 116.6 | 123.4 | 130 ± 0.0 |
| $G$ (GPa) | 76.9 | 77 | 77 | 76.8 | 84.2 | 96 ± 0.0 |
| $E$ (GPa) | 201.5 | 202 | 201 | 201 | 218.5 | |
| $G/B$ | 0.44 | 0.45 | 0.44 | 0.44 | 0.47 | |
| $\nu$ | 0.309 | | 0.308 | 0.308 | | |

[a] This work. [b] Ref. 55. [c] Ref. 56. [d] Ref. 14. [e] Ref. 36. [f] Ref. 37.

Table 2 Calculated lattice parameter, elastic properties, and Poisson's ratio ($\nu$) for $Ni_3(Al,X)$

| | $Ni_3(Al,Ta)$ | $Ni_3(Al,W)$ | $Ni_3(Al,Re)$ | $Ni_3(Al,Mo)$ | $Ni_3(Al,Co)$ | $Ni_3Al$ |
|---|---|---|---|---|---|---|
| $a_0$ (Å) | 3.579 | 3.573 | 3.571 | 3.573 | 3.559 | 3.567 |
| $B$ (GPa) | 180.1 | 182.5 | 183.2 | 181.3 | 179.0 | 175.9 |
| $C_{11}$ (GPa) | 237.5 | 241.9 | 243.9 | 239.7 | 231.0 | 227.9 |
| $C_{12}$ (GPa) | 151.4 | 152.7 | 152.8 | 152.0 | 152.9 | 149.9 |
| $C_{44}$ (GPa) | 122.5 | 126.7 | 127.9 | 124.6 | 118.1 | 120.9 |
| $G$ (GPa) | 80.6 | 83.4 | 84.6 | 82.0 | 75.8 | 76.9 |
| $E$ (GPa) | 210.4 | 217.1 | 220.0 | 213.8 | 199.4 | 201.4 |
| $G/B$ | 0.45 | 0.46 | 0.46 | 0.45 | 0.42 | 0.44 |
| $\nu$ | 0.305 | 0.302 | 0.300 | 0.303 | 0.314 | 0.309 |

according to a previous study[52]). The shear modulus adopts the arithmetic average $G = (G_V + G_R)/2$, where $G_V = (C_{11} - C_{12} + 3C_{44})/5$ and $G_R = 5/(4S_{11} - 4S_{12} + 3S_{44})$ are the Voigt[53] and Reuss[54] bounds, respectively, and $S_{11}$, $S_{12}$ and $S_{44}$ are the elastic compliances.[52] The Young's modulus $E$ and Poisson ratio $\nu$ are calculated as $E = 9GB/(G + 3B)$ and $\nu = (3B - 2G)/(2(3B + G))$, respectively. Our calculated equilibrium lattice parameter for $Ni_3Al$ of 3.567 Å is in good agreement with the experimental data.[55,56] The calculated elastic constants and elastic moduli are also consistent with results from previous experiments[55,56] and DFT calculations.[14,36,37] When substituting the Al-atom with a refractory element, all of the alloying systems except $Ni_3$(Al,Co) have increased lattice parameters, elastic constants and elastic moduli. The increased lattice parameters can be explained by the atomic radius of the X-atom (X = Ta, W, Re and Mo), which was larger than that of the Al-atom. Elastic constants have been considered as primary intrinsic mechanical properties of materials, and they are dominated by the chemical bonding and crystal symmetry. Following analyses of the density of electronic states and charge redistribution will shed light on the strengthening mechanism of these refractory elements on the elastic properties in $\gamma'$-$Ni_3Al$.

Generally, the ideal strength of crystals refers to the first maximum point of the stress–strain curve. The corresponding stress at this point for a material is the maximum ideal tensile strength ($\sigma_{MIT}$). However, the lattice may become mechanically unstable prior to reaching the stress–strain peak in terms of violating the Born criteria of stability under uniaxial load.[51,57] It is important to examine the mechanical stability of a defect-free lattice during the tensile tests as previously verified.[58] The cubic lattice becomes tetragonal, orthorhombic and trigonal under the [001], [110] and [111] directional loading, respectively. The mechanical stability criteria of tetragonal, orthorhombic and trigonal lattices are given by[51,52,59]

$$C_{11} > 0,\ \ C_{44} > 0,\ \ C_{55} > 0,\ \ C_{22} - C_{23} > 0 \text{ and } C_{22} + C_{23} - \frac{2C_{12}^2}{C_{11}} > 0, \quad (3)$$

$$C_{11} > 0,\ C_{22} > 0,\ C_{33} > 0,\ C_{44} > 0,\ C_{55} > 0,\ C_{66} > 0,\ (C_{11} + C_{22} - 2C_{12}) > 0,\ (C_{11} + C_{33} - 2C_{13}) > 0 \text{ and } (C_{22} + C_{33} - 2C_{23}) > 0, \quad (4)$$

and

Table 3 The applied strain configurations employed to calculate the elastic constants of cubic and orthorhombic lattices

| Lattice | Strain configuration | Energy–strain relation |
|---|---|---|
| Cubic phase | (1) $\vec{e} = (\delta, \delta, (1+\delta)^2 - 1, 0, 0, 0)$ | $\Delta E/V_0 = 3(C_{11} - C_{12})\delta^2$ |
| | (2) $\vec{e} = (0, 0, 0, \delta, \delta, \delta)$ | $\Delta E/V_0 = \frac{3}{2}C_{44}\delta^2$ |
| Orthorhombic phase | (3) $\vec{e} = (\delta, 0, 0, 0, 0, 0)$ | $\Delta E/V_0 = \frac{1}{2}C_{11}\delta^2$ |
| | (4) $\vec{e} = (0, \delta, 0, 0, 0, 0)$ | $\Delta E/V_0 = \frac{1}{2}C_{22}\delta^2$ |
| | (5) $\vec{e} = (0, 0, \delta, 0, 0, 0)$ | $\Delta E/V_0 = \frac{1}{2}C_{33}\delta^2$ |
| | (6) $\vec{e} = (\delta, \delta, 0, 0, 0, 0)$ | $\Delta E/V_0 = \frac{1}{2}(C_{11} + 2C_{12} + C_{22})\delta^2$ |
| | (7) $\vec{e} = (\delta, 0, \delta, 0, 0, 0)$ | $\Delta E/V_0 = \frac{1}{2}(C_{11} + 2C_{13} + C_{33})\delta^2$ |
| | (8) $\vec{e} = (0, \delta, \delta, 0, 0, 0)$ | $\Delta E/V_0 = \frac{1}{2}(C_{22} + 2C_{23} + C_{33})\delta^2$ |
| | (9) $\vec{e} = (0, 0, 0, \delta, 0, 0)$ | $\Delta E/V_0 = \frac{1}{2}C_{44}\delta^2$ |
| | (10) $\vec{e} = (0, 0, 0, 0, \delta, 0)$ | $\Delta E/V_0 = \frac{1}{2}C_{55}\delta^2$ |
| | (11) $\vec{e} = (0, 0, 0, 0, 0, \delta)$ | $\Delta E/V_0 = \frac{1}{2}C_{66}\delta^2$ |

$$C_{11} > |C_{12}|,\ (C_{11} + C_{12})C_{33} - 2C_{13}^2 > 0 \text{ and } (C_{11} - C_{12})C_{44} - 2C_{14}^2 > 0, \quad (5)$$

respectively. Herein, the elastic constants are calculated and the mechanical stability examined at every single strain until one of the stable criteria is violated during the tensile test. The stress value at which the mechanical instability occurs is the effective ideal tensile strength ($\sigma_{EIT}$) of a material. To calculate the nine independent elastic constants ($C_{11}$, $C_{22}$, $C_{33}$, $C_{44}$, $C_{55}$, $C_{66}$, $C_{12}$, $C_{13}$ and $C_{23}$) of orthorhombic lattice, sets of distortions (as listed in Table 3) are employed to fit the elastic constants. For the tetragonal lattice ($a \neq b = c$), the number of independent $C_{ij}$ reduce to six as $C_{22} = C_{33}$, $C_{55} = C_{66}$ and $C_{12} = C_{13}$. Thus, for the tetragonal lattice, we employ no. 3, no. 4, no. 6, no. 8, no. 9 and no. 10 strain vectors of Table 3 to fit these six independent elastic constants.

## 3. Results and discussion

Fig. 2(a)–(c) show the calculated stress–strain relationships of $Ni_3(Al,X)$ (X = Ta, W, Re, Mo, Co, and Al) under uniaxial tension along the [001], [110], and [111] directions, respectively. The calculated elastic constants of $Ni_3Al$ at every strain during the [001], [110] and [111] tensile tests are shown in Fig. 3(a)–(c). As shown in Fig. 2(a), the stress of non-doped $Ni_3Al$ continuously increases with increasing strain until it reaches a maximum of 26.27 GPa at a strain of 32%, after which the stress decreases. However, according to Fig. 3(a), the lattice becomes mechanically unstable with $C_{22} = C_{23}$ at a strain of 11% well below its peak point in the stress–strain curve. Thus, the $\sigma_{IT}$ of pure $Ni_3Al$, dictated by $\sigma_{EIT}$, is 12.93 GPa in the [001] direction. The scenario is similar to the [100] tension in a Ni crystal[60] where the lattice bifurcates from tetragonal to an orthorhombic phase ($C_{22} = C_{23}$) prior to its maximum point. When doped with alloying elements, the stress slightly increases before the yield point in the [001] direction. However, all of the doped systems yield at a smaller strain. $Ni_3Al$ doped with Re yields at a strain of 26% and the other alloying systems yield at a strain of 28%. Here, we label the loading at which the Born criteria of stability is violated by the dashed line in Fig. 3(a)–(c). Since the lattice fails as a result of mechanical instability prior to the peak point, $\sigma_{EIT}$ locates the ideal strength during the [001] tensile test. As a result, the $\sigma_{IT}$ values of the alloying systems slightly increase because of minimal enhanced strengthening before the yield point in the [001] direction.

In terms of the [111] direction, the tensile stresses of doped $Ni_3Al$ also yield at a lower strain, as shown in Fig. 2(c). The lattice becomes mechanically unstable at a strain of 19% while the $\sigma_{MIT}$ of $Ni_3Al$ is reached at a strain of 22% according to Fig. 3(c). Therefore, the ideal tensile strength of pure $Ni_3Al$ is 25.55 GPa in the [111] direction. Here, it is important to state that the supercell as shown in Fig. 1(b) was employed and treated as an orthorhombic lattice to calculate the elastic constants during the [111] tension. Certainly, the supercell still possesses six independent elastic constants, $C_{ij}$, as shown in Fig. 3(c). Unlike the failure in the [001] tension, the mode of failure for the [111] tension is $C_{44} = 0$. Furthermore, the BCT stability zone (the mechanical stability zone in terms of Born criteria) includes the peak point from the $\sigma$–$\varepsilon$ curve for alloying systems (as shown in Fig. 2(c)). Therefore, the $\sigma_{IT}$ of the substitutional systems slightly decrease in the [111] direction.

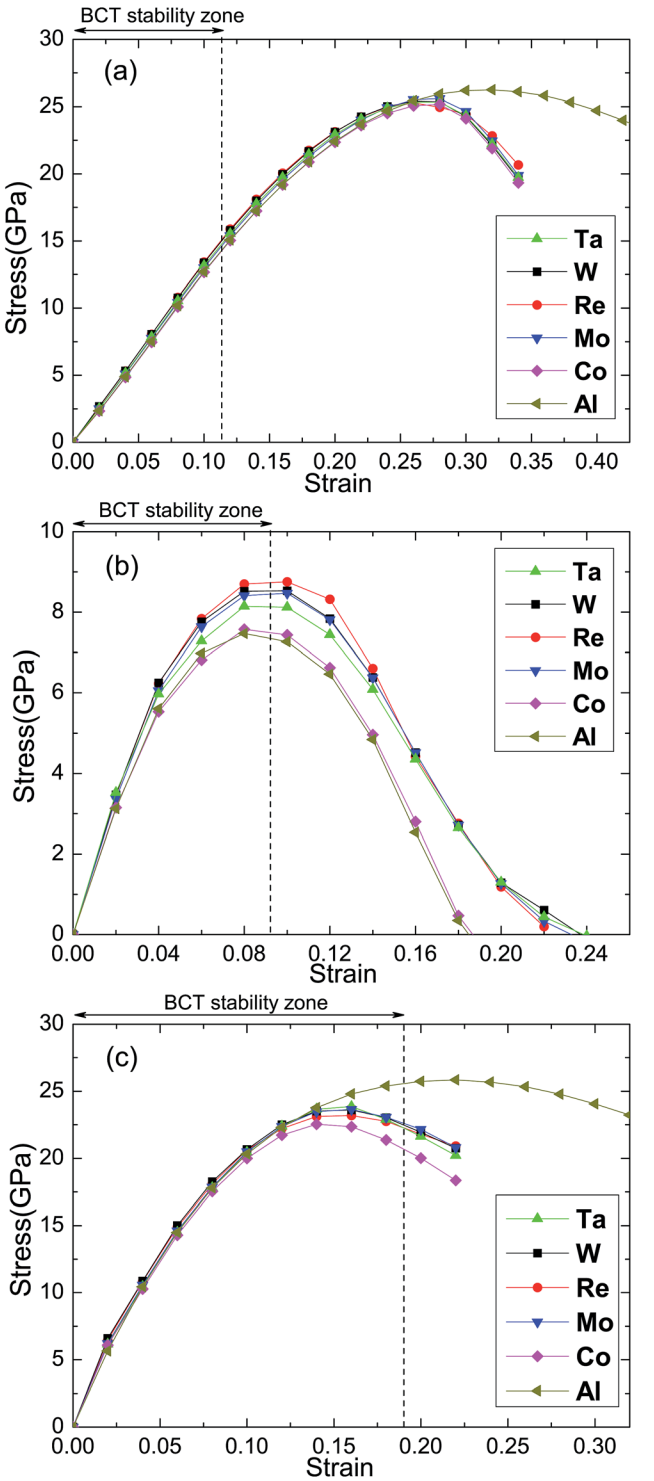


Fig. 2 (a)–(c) Stress as a function of tensile strain for $Ni_3(Al,X)$ under [001], [110] and [111] tension, respectively. X = Ta, W, Re, Mo, and Al, where X = Al represents non-doped $Ni_3Al$. The vertical dashed lines mark the loading at which the lattice becomes unstable in terms of Born criteria.

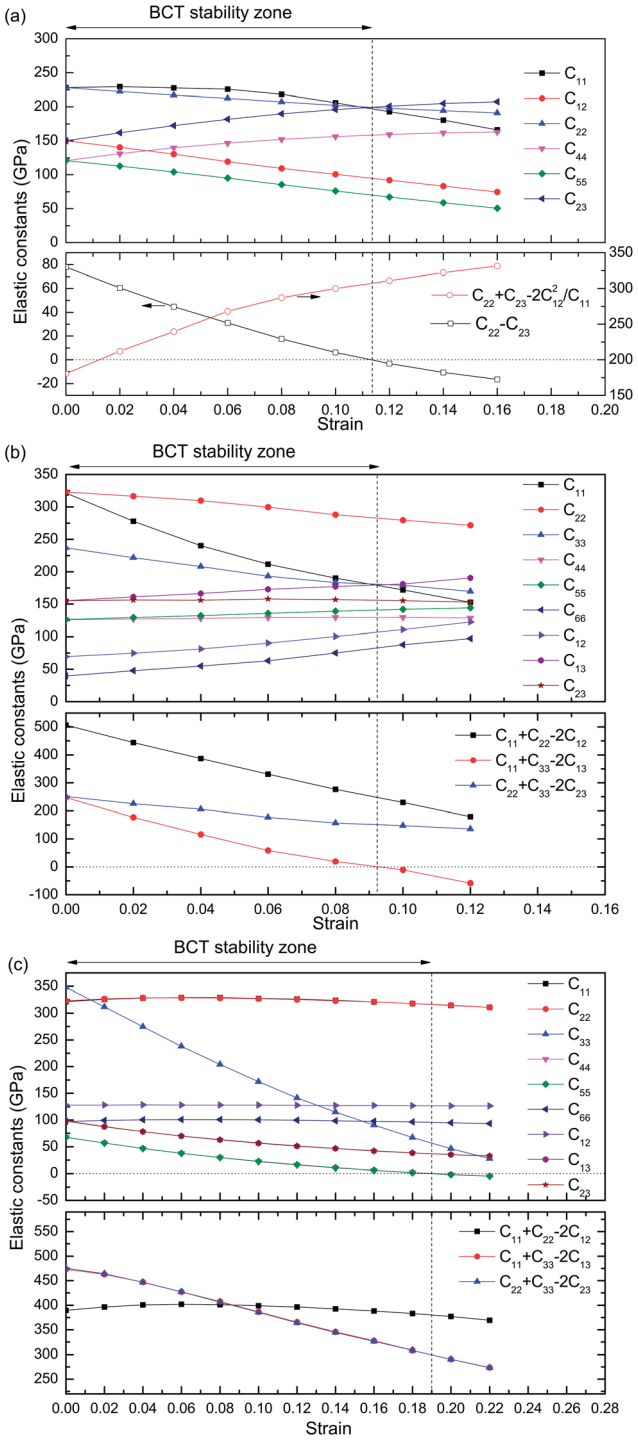


Fig. 3 (a)–(c) Elastic constants (upper panel) and corresponding Born criteria of stability (lower panel) of $Ni_3Al$ during the [001], [110] and [111] tensile tests, respectively. The vertical dashed lines mark the loading at which the Born criteria of stability is violated.

Taking into consideration the Born criteria of stability during uniaxial load, Table 4 lists the $\sigma_{IT}$ values and corresponding strains in all of the calculated directions. Note that the calculated $\sigma_{MIT}$ of non-doped $\gamma'$-$Ni_3Al$ is in agreement with the results of Wang *et al.*[61] who observed that the addition of Re can improve $\sigma_{MIT}$ of $\gamma'$-$Ni_3Al$ by 1% and 6% in the [001] and [111] directions, respectively. The different models used in their study and the present work may be responsible for the discrepancy. Here, we used single-impurity models and the distance between impurities is farther than the fifth nearest neighbor. Such supercells can avoid interactions between doping atoms during tensile tests. Furthermore, the stress–strain curves in Fig. 2(a)–(c) are continuous and smooth, which indicates the reliability of the method used in this study.

Table 4 Calculated ideal tensile strength $\sigma_{IT}$ with the corresponding engineering strain $\varepsilon$ for $Ni_3(Al,X)$ in the [001], [110] and [111] directions

| | [001] | | [110] | | [111] | |
|---|---|---|---|---|---|---|
| System | $\sigma_{IT}$ (GPa) | $\varepsilon$ | $\sigma_{IT}$ (GPa) | $\varepsilon$ | $\sigma_{IT}$ (GPa) | $\varepsilon$ |
| $Ni_3(Al,Ta)$ | 13.42 | 0.11 | 8.14 | 0.08 | 23.89 | 0.16 |
| $Ni_3(Al,W)$ | 13.64 | 0.11 | 8.52 | 0.09 | 23.61 | 0.16 |
| $Ni_3(Al,Re)$ | 13.71 | 0.11 | 8.73 | 0.09 | 23.2 | 0.16 |
| $Ni_3(Al,Mo)$ | 13.28 | 0.11 | 8.43 | 0.09 | 23.64 | 0.16 |
| $Ni_3(Al,Co)$ | 12.98 | 0.11 | 7.57 | 0.08 | 22.53 | 0.14 |
| $Ni_3Al$ | 12.93 | 0.11 | 7.20 | 0.08 | 25.55 | 0.19 |

The stress–strain relationship in the [110] direction is different from those in the [001] and [111] directions. As shown in Fig. 2(a)–(c), the [001] and [111] directions can be considered as strong orientations with $\sigma_{IT}$ as large as 12 GPa. However, the [110] direction is obviously the weakest direction for $\gamma'$-$Ni_3Al$ with $\sigma_{IT}$ yielding only 7.2 GPa. In the $C_{11} + C_{33} = 2C_{13}$ mode (as shown in Fig. 3(b)), the lattice remains true to the Born criteria of stability until a strain of 9%, and thereafter fails upon increasing strain in the [110] tension for non-doped, Ta-doped and Co-doped systems. For $Ni_3(Al,W)$, $Ni_3(Al,Re)$ and $Ni_3(Al,Mo)$, the point at which mechanical instability occurs is immediately prior to the yield point. Addition of alloying elements X (X = Ta, W, Re, and Mo) can considerably improve the tensile stress and $\sigma_{IT}$ in the [110] direction, and Re exhibits the greatest improvement, as shown in Fig. 2(b). Note that doping with Co has a negligible effect on the stress of the $\gamma'$-

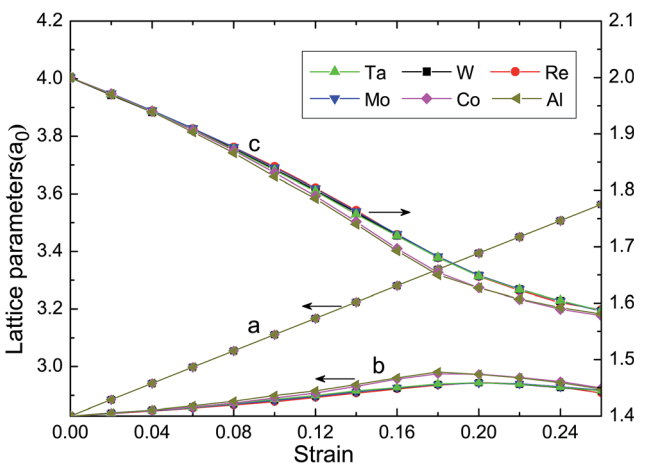


Fig. 4 Variation of the lattice parameters of $Ni_3(Al,X)$ during the [110] tensile test. X = Ta, W, Re, Mo, Co, and Al, where X = Al represents non-doped $Ni_3Al$.

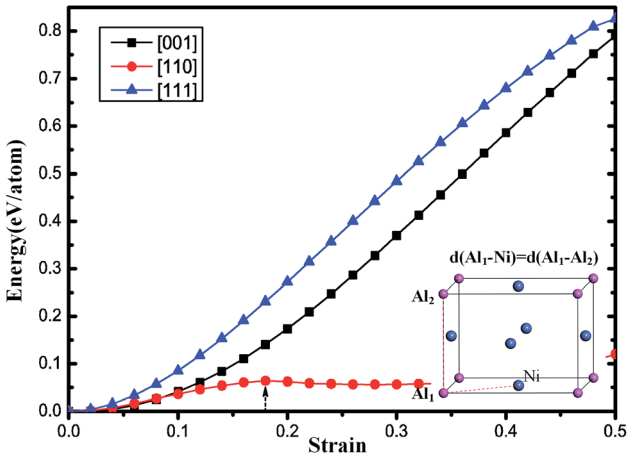


Fig. 5 Response of the energy of $L1_2$-$Ni_3Al$ to strain under [001], [110], and [111] tensile deformation. The dashed arrows indicate the onset strain for the second zero-stress and the inset shows the structure at this point.

$Ni_3Al$ phase. As listed in Table 4, the ability of the alloying elements to increase the $\sigma_{IT}$ are in the order: Re > W > Mo > Ta > Co. Compared with pure $Ni_3Al$, the $\sigma_{MIT}$ of $Ni_3$(Al,Re) improves from 7.2 to 8.75 GPa, an increase of 22%. Wang *et al.*[61] found that addition of Re can increase $\sigma_{IT}$ by 51% in the [110] direction. This larger increase is because of the higher alloying element concentration in their model.

According to the above results in relation to the mechanical stability in terms of Born criteria examinations, the $\sigma_{IT}$ of $L1_2$-$Ni_3Al$ along the [001], [110] and [111] directions are determined to be 12.93 GPa, 7.20 GPa and 25.55 GPa, respectively. The [110] orientation is the weakest uniaxial tensile direction. It is important to mention here that we do not perform phonon calculations to verify the phonon stability during the tensile processes. In fact, phonon-induced instabilities may occur significantly prior to the stress–strain peak, similar to the scenario undergoing during the tension and $\langle 112 \rangle \{111\}$ shear for an Al crystal.[8] Consequently, our predictions may overestimate the ideal strength.

The effect of alloying elements on $\sigma_{IT}$ of $Ni_3Al$ exhibits obvious directionality. The orientation dependence of the strengthening mechanism arises from interatomic interactions that vary significantly in different directions in $Ni_3Al$. Analysis of charge redistribution will reveal these interactions between impurities and host atoms. Impurities have the strongest effect on the [110] direction. Hence, we will highlight the electronic mechanism of alloying elements during [110] tensile deformation in later analyses.

The dependence of the lattice parameters under [110] uniaxial strain is shown in Fig. 4. With uniformly increasing tensile strain (*i.e.*, increasing lattice parameter $a$), $c$ decreases and $b$ remains almost constant. When the supercell of pure $Ni_3Al$ is deformed by 18%, the $c$ lattice parameter is equal to half of $a$ (see Fig. 4). Therefore, the distance between an Al atom and the first nearest neighbor (FNN) Ni atom along the [110]

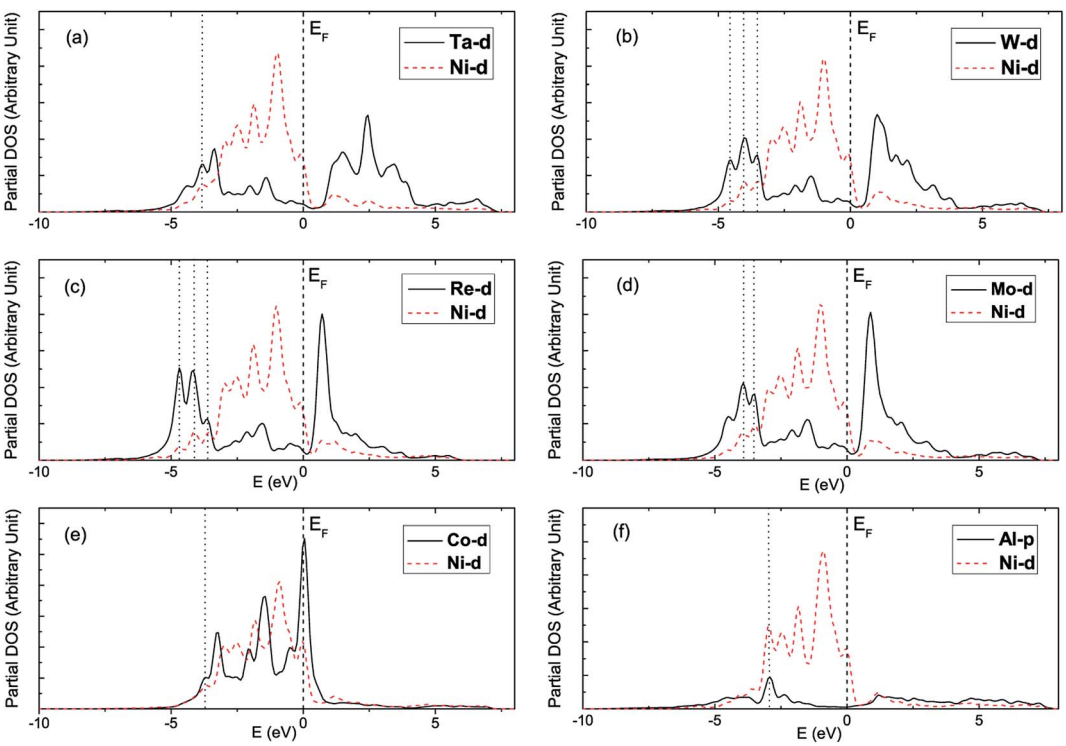


Fig. 6 (a)–(e) d-Orbital partial density of states (DOS) for doping an X atom and its first nearest neighbor (FNN) Ni-atom along the [110] direction in 64-atom $Ni_3$(Al,Ni) at $\varepsilon = 0.00$ (X = Ta, W, Re, Mo and Co). (f) Partial DOS of the central Al atom and its FNN Ni atom in pure $Ni_3Al$ at $\varepsilon = 0.00$. The dashed and dotted lines indicate the Fermi level and the locations of resonant hybridization peaks, respectively.

 

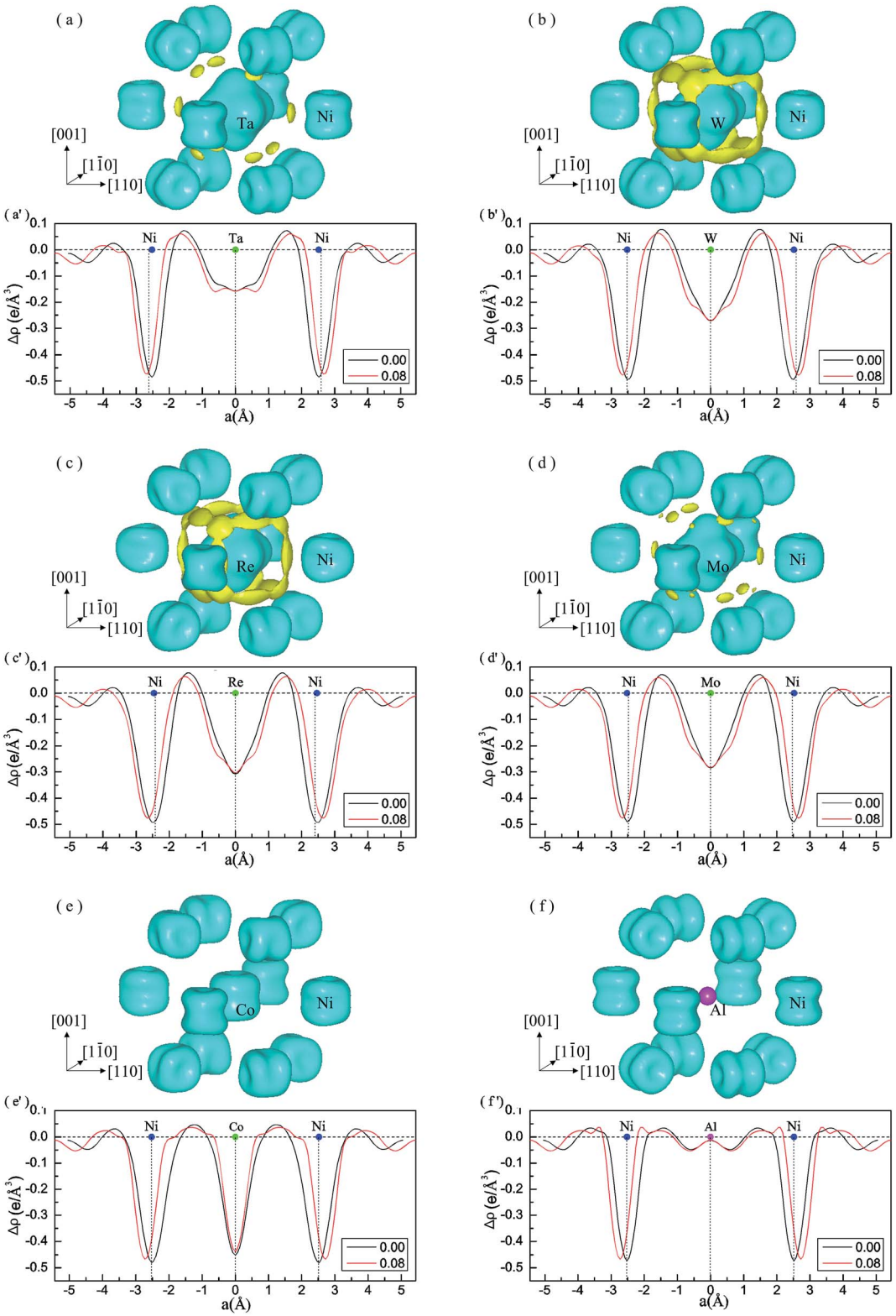


Fig. 7 (a)–(f) Charge density difference (isovalues ± 0.0672 e Å$^{-3}$) in real space at zero strain. The yellow (cyan) isosurface denotes charge accumulation (depletion). (a′)–(f′) $\Delta\rho$ along the [110] direction at $\varepsilon = 0.00$ and $\varepsilon = 0.08$ during the [110] tensile test.

direction is equivalent to the distance between nearest Al atoms along the [001] direction, as shown in the inset of Fig. 5. Accordingly, at this point, the response of the energy under [110] tension has a saddle point, as shown in Fig. 5, which indicates that the new triclinic structure is an unstable "phase". Consequently, the stress reaches the second zero-stress point

according to eqn (1) and attains its maximum at an early strain of about half of 18%, which is consistent with the stress–strain relationship shown in Fig. 2(b). In contrast to the [110] loading direction, the energies monotonically increase between $\varepsilon = 0.00$ and $\varepsilon = 0.50$ under tension along the [001] and [111] directions (Fig. 5). It can be concluded that the $\sigma_{MIT}$ of the [110] tension being the lowest $\sigma_{MIT}$ among the three characteristic directional loading is an intrinsic characteristic of the $L1_2$ structure (space group: $Pm\bar{3}m$).

Fig. 4 also shows the influence of alloying elements on variation of the lattice parameters during the [110] tensile test. Doping with Co has a negligible effect on variation of the lattice parameters. Fig. 4 shows that Ta, W, Re, and Mo can considerably decrease the rate of variation of the $b$ and $c$ lattice parameters of $\gamma'$-$Ni_3Al$. It is expected that Ta, W, Re, and Mo can improve the mechanical strength and deformation resistance of alloys. These results are consistent with the stress–strain relationships (Fig. 2(b)), and agree well with previous experiments.[38,40,62,63]

Although Co has a negligible effect on the stress of $\gamma'$-$Ni_3Al$, the other doping elements (*i.e.*, Ta, W, Re, and Mo) can enhance $\sigma_{IT}$ in the weakest tensile direction. To reveal the strengthening mechanism, we investigated the density of states (DOS) of these alloying systems. Fig. 6(a)–(e) show the d-orbital partial DOS of doping element X and its FNN Ni atom along the [110] direction. The partial DOS of pure $Ni_3Al$ are also plotted in Fig. 6(f) for comparison. As shown in Fig. 6(a)–(e), all of the alloying elements except Co have a prominent feature: the noticeable bonding and antibonding region of X-d (X = Ta, W, Re, and Mo) orbitals is well separated by a deep valley near the Fermi level. This feature indicates that these alloying elements can stabilize the system by substituting for the Al atom in $\gamma'$-$Ni_3Al$.[64] Additionally, there are strong interactions between X and the host atom Ni in the doping systems by d–d hybridization (see Fig. 6). Here, we indicate the resonant hybridization peaks by dotted lines in Fig. 6(a)–(f). Interaction between Re and Ni shows the greatest hybridization, followed by W–Ni, Mo–Ni, and Ta–Ni. The partial DOS of $Ni_3$(Al,Co) behaves in a different way: the Fermi level is located at the peak of the Co-d DOS and the interaction between Co-d and Ni-d is weak. It is expected that Co will improve the ductility of $Ni_3Al$ rather than the mechanical strength. Consequently, addition of Co has a negligible effect on the response of the tensile stress to strain during the [110] deformation test (see Fig. 2(b)).

We next investigated the charge density difference ($\Delta\rho$) of $Ni_3$(Al,X) in the process of tensile deformation. Charge redistribution induced by impurities can directly reflect the bonding nature between alloying atoms and host atoms. The $\Delta\rho$ between the impurity atom and its FNN host atoms (twelve Ni atoms) in real space and $\Delta\rho$ along the [110] direction in [110] tensile deformation are shown in Fig. 7. Electrons flow from both Ni and X (X = Ta, W, Re, and Mo) atoms into covalent-like Ni–X bonds (Fig. 7(a′)–(d′)). Charge accumulation shows robust directionality, mainly appearing along the ⟨110⟩ direction for X-doped systems (X = Ta, W, Re, and Mo), as shown in Fig. 7(a)–(d). This suggests that interactions between these impurities and Ni atoms exhibit strong directionality, which is the origin of their directional strengthening effect on the $\sigma_{IT}$ in the $\gamma'$-$Ni_3Al$ phase.

Moreover, $\Delta\rho$ is quite different dependent upon the alloying system. As shown in Fig. 7(b) and (c), $\Delta\rho$ in Re-doped and W-doped systems exhibit similar features. However, although Ta, W and Re are the adjacent element in the sixth period, Ta has a considerably weaker effect than W and Re (see Table 4) on improving $\sigma_{IT}$ in the $\gamma'$-$Ni_3Al$ phase. Fig. 7(a–c) reveals the origin of the strengthening effect. Charge accumulation in the W-doped and Re-doped systems is stronger than in the Ta-doped system. Interaction of W–Ni and Re–Ni can effectively improve the mechanical strength, which agrees with experimental investigations.[38,62] As shown in Fig. 7(d), $\Delta\rho$ in the Mo-doped system shows stronger charge accumulation than the Ta-doped system but weaker than the W-doped and Re-doped system, which is consistent with previous calculations of the ideal tensile stress (Table 4). Unlike the other alloying systems, the missing charge accumulation at the isovalue of 0.0672 e $Å^{-3}$ in the Co-doped system (Fig. 7(e)) suggests more metallic bonding character between Co and FNN Ni atoms. It is expected that doping with Co can improve the malleability and ductility in nickel-based alloys rather than the mechanical strength. Al has an electronic structure of $3s^2 3p^1$ with only three valence electrons, which greatly contributes to it having the smallest $\sigma_{IT}$ among all of the investigated systems. Accordingly, compared with alloying elements, $\Delta\rho$ near the Al atom is very small in pure $Ni_3Al$ (see Fig. 7(f′)). In all of the systems, with increasing tensile strain, the distances between atoms along the [110] direction increases and $\Delta\rho$ becomes smoother, as shown in Fig. 7(a′)–(f′).

# 4. Conclusions

We have investigated the influence of alloying elements on the ideal tensile strength and charge redistribution of $\gamma'$-$Ni_3Al$ using first-principles calculations. Our results show that through examinations of mechanical stability in terms of Born criteria for all calculated orientations, the $\sigma_{IT}$ of $L1_2$-$Ni_3Al$ along [001], [110] and [111] directions is determined to be 12.93 GPa, 7.20 GPa and 25.55 GPa, respectively. Doping with Ta, W, Re, Mo, and Co slightly increases $\sigma_{IT}$ along the [001] direction and decreases $\sigma_{IT}$ in the [111] tension, however, $\sigma_{IT}$ along the [110] direction is increased by 0.94, 1.32, 1.53, 1.23, and 0.37 GPa, respectively. The directional strengthening effect arises from directional interactions between impurities and host atoms. Analysis of the lattice parameters during the tensile tests shows that W, Re, Mo, and Ta can improve the deformation resistance of nickel-based alloys and Co has a negligible effect on variation of the lattice parameters. The DOS of the alloying atom and its FNN Ni-atom along the [110] orientation in the 64-atom supercell at zero strain, and $\Delta\rho$ of $Ni_3$(Al,X) during the [110] tensile deformation were also calculated. The d-orbital partial DOS indicate that Ta, W, Re, and Mo can enhance the structural stability of the $Ni_3Al$ phase when substituted for an Al atom, and interactions between impurities and host atoms are by d–d hybridization. Charge redistribution of these alloying systems shows that charges mainly gather along the ⟨110⟩ direction for X-doped systems, and charge accumulation in the W-doped and

 

Re-doped systems is the strongest, followed by Mo-doped, Ta-doped, and Co-doped alloys. Our results are of importance to reveal the strengthening mechanisms of Ta, W, Mo, and Co in the $\gamma'$-$Ni_3Al$ phase for tensile deformation, which has not previously been investigated using *ab initio* calculations.

## Acknowledgements

We are grateful to B. K. Lu, X. X. Yu and P. F. Guan for beneficial discussions. This work was supported by the National Basic Research Program of China (Grant No. 2011CB606402). The simulations were performed using the "Explorer 100" cluster system of Tsinghua National Laboratory for Information Science and Technology, Beijing, China.

## References

1 A. Kelly and N. H. Macmillan, *Strong Solids*, Clarendon Press, Oxford, 3rd edn, 1986.
2 D. Roundy, C. R. Krenn, M. L. Cohen and J. W. Morris Jr, *Phys. Rev. Lett.*, 1999, **82**, 2713.
3 A. Gouldstone, H. J. Koh, K. Y. Zeng, A. E. Giannakopoulos and S. Suresh, *Acta Mater.*, 2000, **48**, 2277.
4 C. R. Krenn, D. Roundy, M. L. Cohen, D. C. Chrzan and J. W. Morris Jr, *Phys. Rev. B: Condens. Matter Mater. Phys.*, 2002, **65**, 134111.
5 M. Šob, M. Friák, D. Legut, J. Fiala and V. Vitek, *Mater. Sci. Eng., A*, 2004, **387–389**, 148.
6 M. Černý and J. Pokluda, *Phys. Rev. B: Condens. Matter Mater. Phys.*, 2010, **82**, 174106.
7 D. Roundy, C. R. Krenn, M. L. Cohen and J. W. Morris Jr, *Philos. Mag. A*, 2001, **81**, 1725.
8 D. M. Clatterbuck, C. R. Krenn, M. L. Cohen and J. W. Morris Jr, *Phys. Rev. Lett.*, 2003, **91**, 135501.
9 S. Ogata, J. Li and S. Yip, *Science*, 2002, **298**, 807.
10 D. M. Clatterbuck, D. C Chrzan and J. W Morris Jr, *Acta Metall.*, 2003, **51**, 2271.
11 S. Ogata, J. Li, N. Hirosaki, Y. Shibutani and S. Yip, *Phys. Rev. B: Condens. Matter Mater. Phys.*, 2004, **70**, 104104.
12 Y. L. Liu, Y. Zhang, H. B. Zhou, G. H. Lu and M. Kohyama, *J. Phys.: Condens. Matter*, 2008, **20**, 335216.
13 T. Li, J. W. Morris Jr and D. C. Chrzan, *Phys. Rev. B: Condens. Matter Mater. Phys.*, 2004, **70**, 054107.
14 Y. J. Wang and C. Y. Wang, *Appl. Phys. Lett.*, 2009, **94**, 261909.
15 C. Kocer, N. Hirosaki and S. Ogata, *Phys. Rev. B: Condens. Matter Mater. Phys.*, 2003, **67**, 035210.
16 X. L. Wang, K. Bao, F. B. Tian, X. Meng, C. B. Chen, B. W. Dong, D. Li, B. B. Liu and T. Cui, *J. Chem. Phys.*, 2010, **133**, 044512.
17 X. X. Zhang, Y. C. Wang, J. Lv, C. Y. Zhu, Q. Li, M. Zhang, Q. Li and Y. M. Ma, *J. Chem. Phys.*, 2013, **138**, 114101.
18 F. Gao, J. Zhang and Z. Li, *RSC Adv.*, 2014, **4**, 32345.
19 M. J. Xing, B. H. Li, Z. T. Yu and Q. Chen, *RSC Adv.*, 2016, **6**, 32740.
20 X. L. Hu, Y. Zhang, G. H. Lu and T. Wang, *J. Phys.: Condens. Matter*, 2009, **21**, 025402.
21 W. Xu, Y. Wang, C. Wang, X. Liu and Z. K. Liu, *Scr. Mater.*, 2015, **100**, 5.
22 G. H. Lu, Y. Zhang, S. Deng, T. Wang, M. Kohyama, R. Yamamoto, F. Liu, K. Horikawa and M. Kanno, *Phys. Rev. B: Condens. Matter Mater. Phys.*, 2006, **73**, 224115.
23 D. Yin, Y. Yang, X. Peng, Y. Qin and Z. Wang, *Ceram. Int.*, 2014, **40**, 14453.
24 S. L. Shang, W. Y. Wang, Y. Wang, Y. Du, J. X. Zhang, A. D. Patel and Z. K. Liu, *J. Phys.: Condens. Matter*, 2012, **24**, 155402.
25 X. Wu and C. Wang, *RSC Adv.*, 2016, **6**, 20551.
26 C. T. Sims, N. S. Stoloff and W. C. Hagel, *Superalloy II*, John Wiley & Sons, New York, 1987.
27 R. C. Reed, *The Superalloys: Fundamentals and Applications*, Cambridge University Press, New York, 2006.
28 E. A. Loria, *Superalloy 718: Metallurgy and Applications*, TMS, Warrendale, PA, 1989.
29 H. P. Karnthaler, E. T. Mühlbacher and C. Rentenberger, *Acta Mater.*, 1996, **44**, 547.
30 T. M. Pollock and S. Tin, *J. Propul. Power*, 2006, **22**, 361.
31 R. C. Reed, T. Tao and N. Warnken, *Acta Mater.*, 2009, **57**, 5898.
32 S. L. Liu, C. Y. Wang and Tao Yu, *RSC Adv.*, 2015, **5**, 52473.
33 C. Y. Geng, C. Y. Wang and T. Yu, *Acta Mater.*, 2004, **52**, 5427.
34 C. Jiang and B. Gleeson, *Scr. Mater.*, 2006, **55**, 433.
35 Y. J. Wang and C. Y. Wang, *J. Appl. Phys.*, 2008, **104**, 013109.
36 Q. Wu and S. Li, *Comput. Mater. Sci.*, 2012, **53**, 436.
37 A. Kumar, A. Chernatynskiy, M. Hong, S. R. Phillpot and S. B. Sinnott, *Comput. Mater. Sci.*, 2015, **101**, 39.
38 M. V. Nathal and L. J. Ebert, *Metall. Trans. A*, 1985, **16**, 1863.
39 P. Carron and T. Khan, *Aerosp. Sci. Technol.*, 1999, **3**, 513.
40 E. Fleischmann, M. K. Miller, E. Affeldt and U. Glatzel, *Acta Mater.*, 2015, **87**, 350.
41 C. Y. Wang, S. Y. Liu and L. G. Han, *Phys. Rev. B: Condens. Matter Mater. Phys.*, 1990, **41**, 1359.
42 A. V. Ruban and H. L. Skriver, *Phys. Rev. B: Condens. Matter Mater. Phys.*, 1997, **55**, 856.
43 A. V. Ruban, V. A. Popov, V. K. Portnoi and V. I. Bogdanov, *Philos. Mag.*, 2014, **94**, 20.
44 P. Hohenberg and W. Kohn, *Phys. Rev.*, 1964, **136**, B864.
45 W. Kohn and L. J. Sham, *Phys. Rev.*, 1965, **140**, A1133.
46 G. Kresse and J. Furthmüller, *Phys. Rev. B: Condens. Matter Mater. Phys.*, 1996, **54**, 11169.
47 G. Kresse and J. Joubert, *Phys. Rev. B: Condens. Matter Mater. Phys.*, 1999, **59**, 1758.
48 J. P. Perdew, K. Burke and M. Ernzerhof, *Phys. Rev. Lett.*, 1996, **77**, 3865.
49 H. J. Monkhorst and J. D. Pack, *Phys. Rev. B: Solid State*, 1976, **13**, 5188.
50 F. D. Murnaghan, *Proc. Natl. Acad. Sci. U. S. A.*, 1944, **30**, 244.
51 F. Milstein, *Phys. Rev. B: Solid State*, 1971, **3**, 1130.
52 J. F. Nye, *Physical Properties of Crystals*, Clarendon Press, Oxford, 1985.
53 W. Voigt, *Lehrbuch der Kristallphysik*, Teubner Press, Leipzig, 1928.
54 A. Reuss, *Z. Angew. Math. Mech.*, 1929, **9**, 49.
55 F. Kayser and C. Stassis, *Phys. Status Solidi A*, 1981, **64**, 335.

56 M. J. Mehl, B. M. Klein and D. A. Papaconstantopoulos, *Intermetallic Compounds: Principles and Practice*, Wiley, New York, 1995.
57 R. Hill and F. Milstein, *Phys. Rev. B: Solid State*, 1977, **15**, 3087.
58 A. Breidi, S. G. Fries and A. V. Ruban, *Phys. Rev. B*, 2016, **93**, 144106.
59 Z. J. Wu, E. J. Zhao, H. P. Xiang, X. F. Hao, X. J. Liu and J. Meng, *Phys. Rev. B: Condens. Matter Mater. Phys.*, 2007, **76**, 054115.
60 F. Milstein and B. Farber, *Phys. Rev. Lett.*, 1980, **44**, 277.
61 Y. J. Wang and C. Y. Wang, *Scr. Mater.*, 2009, **61**, 197.
62 A. C. Yeh and S. Tin, *Scr. Mater.*, 2005, **52**, 519.
63 M. Fahrmann, W. Hermann, E. Fahrmann, A. Boegli, T. M. Pollock and H. G. Sockel, *Mater. Sci. Eng., A*, 1999, **260**, 212.
64 J. H. Xu, T. Oguchi and A. J. Freeman, *Phys. Rev. B: Condens. Matter Mater. Phys.*, 1987, **36**, 4186.